IOP Publishing Superconductor Science and Technology
Supercond. Sci. Technol. 31 (2018) 055011 (7pp) https://doi.org/10.1088/1361-6668/aab5fd

Magnetic losses of commercial *RE*BCO coated conductors in the low frequency range

G De Marzi[1], G Iannone[2] and U Gambardella[2]

[1] ENEA, FSN Department, Via Enrico Fermi 45, I-00044 Frascati, Italy
[2] INFN-Napoli section, Salerno Group, University of Salerno, I-84084 Fisciano, Italy

E-mail: gianluca.demarzi@enea.it

Received 10 December 2017, revised 8 March 2018
Accepted for publication 12 March 2018
Published 5 April 2018

Abstract

We have investigated the frequency dependence of the magnetic losses of different 2 G commercial *RE*BCO coated-conductor tapes in the low frequency range ~1–10 mHz of applied magnetic field at 5 and 77 K. We explored high field range, well above the penetration field, with fields applied perpendicularly to the flat surface. We found that the in-field hysteresis losses increase with increasing frequencies in all the investigated high-temperature superconductor (HTS) tapes, following a power-law dependence. An electromagnetic 2D finite element method model, based on *H*-formulation, has also been implemented, in which the frequency dependence of the hysteretic loss is computed taking into account the measured power-law $E(J)$ characteristic for the electric field, and the experimental $J_c(B)$. Experimental and numerical findings are in very good agreement, so an extrapolation to higher ramp rate values is possible, thus providing a useful basis for the assessment of the hysteresis losses in fusion and accelerator HTS magnets.

Keywords: AC losses, hysteresis losses, HTS coated conductors, vibrating sample magnetometer

(Some figures may appear in colour only in the online journal)

1. Introduction

Second generation coated conductors (CCs) based on *RE*BCO (*RE* = rare earth) high-temperature superconductors (HTSs) are nowadays being commercialized by several companies worldwide. CCs are now being produced in lengths of several hundred meters, with outstanding current density capacity, which can be tailored to specific power or magnet applications, as well as to specific operating conditions. Such versatile CC availability on the market has triggered the design and realization of a number of HTS device demonstrators [1]; among them, several devices (e.g., dipole magnets, transmission and distribution cables, low pass filter inductors, fault current limiters) have been especially designed for working under AC operating conditions. However, it is well known that the AC performance of such superconducting devices can be greatly affected by the high AC losses generated in variable field and/or transport current; this is particularly true when the time-varying magnetic fields are applied perpendicularly to the flat surface of the tape [2]. Moreover, large dissipations can also occur in typical DC applications: for example, fusion or accelerator magnets undergo transient AC losses when the currents are ramped to their target values. In light of the above, a superconducting device's design should be oriented towards low AC losses performance.

Generally, we can approximate the AC loss in a superconducting device, Q_{AC}, as the sum of three contributions:

$$Q_{AC} = Q_h + Q_e + Q_c, \quad (1)$$

where Q_h is the hysteresis loss in the superconductor due to the flux pinning, Q_e is the eddy current loss originating from induced currents flowing in normal conducting parts, and Q_c is the coupling loss due to the currents flowing across different superconducting portions through normal conducting interconnecting parts. In the mHz frequency range, Q_h is the dominant contribution, whereas both Q_e and Q_c have a marginal role and can be neglected [3]. In the critical state model (CSM) for the electrodynamics of a superconductor, based on the Bean's approximation [4], Q_h is independent of frequency because the

Table 1. Geometrical characteristics, I_c values and n-index of the samples cut from commercial CCs.

CC tape	Width[a] (mm)	Length[a] (mm)	I_c (A)[b] @ sf, 77 K	n-index[b] @ 3 T, 77 K	n-index[b] @ 10 T, 5 K
SuNAM (HCN-04100)	4.0	5.0	160.9	7.3	34
SuperOx	4.0	5.0	71.8	6.6	37.3
SuperPower (SCS4050-AP)	4.0	3.0	112.5	9.5	47.8

[a] Sample geometry for magnetization measurements.
[b] From transport measurements.

penetration field does not depend upon its variation rate. Furthermore in the particular geometry of a thin superconducting strip, with the magnetic field oriented perpendicularly to the strip flat surface, Brandt and Indenbom found an analytical expression for the magnetization loss per volume per cycle [5]:

$$Q_h = \frac{\mu_0 J_c^2 w d}{\pi}\left\{2\ln\left[\cosh\left(\frac{\pi B_a}{\mu_0 J_c d}\right)\right] - \frac{\pi B_a}{\mu_0 J_c d}\tanh\left(\frac{\pi B_a}{\mu_0 J_c d}\right)\right\}, \quad (2)$$

where: μ_0 is the vacuum permeability; w and d are the strip's width and thickness, respectively; J_c represents the critical current density; and B_a is the applied field.

As it can be inferred from equation (2), in the framework of the CSM there is no frequency dependence in the magnetic AC loss per cycle. This constitutes a good approximation for hard superconductors, as their E–J relationship is very steep (ideally infinite) at the superconducting transition. When this condition is not fulfilled as in the case of HTS superconductor, the CSM is no longer valid, and to accurately describe the electrodynamics of the superconductor it is necessary to consider the power-law E–J characteristic:

$$E = E_c\left(\frac{J}{J_c}\right)^n \quad (3)$$

in which the electric field criterion E_c is usually set to 10^{-4}–10^{-5} V m^{-1}. The hysteresis AC loss can be calculated by integrating the product of the local electric field and current density over a cycle:

$$Q_h = \oint \boldsymbol{E}\cdot\boldsymbol{J}\,dt. \quad (4)$$

As described by Banno and Amemiya [6], in the limit $B_a \gg B_p$, where B_p is the penetration field, an analytical expression for the losses can be obtained by including equation (3) in (4), and frequency dependence may be found as:

$$Q_h(T, B, f) \propto f^{1/n} \quad (5)$$

with T being the temperature.

Thus, the hysteresis loss is found to increase with increasing frequency f proportionally to $(f)^{1/n}$, where n is the exponent describing the steepness of the E–J curve.

An experimental evidence on such a frequency dependence was reported in [3]: for the magnetic AC loss in 2 G tapes, Q_h follows an $f^{1/n}$ law at 77 K sweeping the magnetic field B_a up to 0.15 T, around zero, with a frequency up to 350 mHz.

In this paper we present measurements of Q_h on three 4 mm wide CC commercial tapes, manufactured by different producers. The hysteretic AC losses have been measured at 77 K and 5 K sweeping the magnetic field $B_a \pm 0.6$ T, around 3 T and 10 T, respectively, with a ramp rates from 0.05 to 1 T min^{-1}. In the following we deal with field ramp rate $\dot{B}$ instead of f, which is related to $\dot{B}$ by $f = \frac{\dot{B}}{2(B_{max}-B_{min})} = \frac{\dot{B}}{2\Delta B}$, B_{max}, B_{min} being the maximum and minimum value of the magnetic field applied in the cycle, respectively.

Complete characterizations of E–J curves and $J_c(B)$ curves have been also performed on the samples.

To support our Q_h experimental results, finite element method (FEM) calculations were carried out. We used the H-formulation [7], for thin superconducting strips subjected to varying magnetic fields, with the aim to provide a useful tool for extending the computation to faster ramp rates, and/or supporting the study of more complex geometries like coils and magnets.

2. Experimental and computational details

2.1. Samples

The samples are rectangular specimens cut from commercial CC tapes provided by three different manufacturers which use different manufacturing technologies. In SuperOx tapes, the superconducting layer was grown by pulsed laser deposition onto an ion beam assisted deposition (IBAD) substrate. The active layer of SuNAM HCN-04100 was deposited by the reactive co-evaporation by deposition and reaction (RCE-DR) technique onto an Hastelloy substrate. Finally, SuperPower SCS4050-AP had IBAD templates with the YBCO layer made by metal organic chemical vapor deposition, and it is the only one containing artificial pinning centers (APCs) for the enhancement of the in-field properties. The main parameters of the investigated samples are summarized in table 1.

2.2. Measurements

Critical currents, I_c, have been measured by DC transport technique in liquid helium and liquid N_2 bath at different applied magnetic fields up to 14 T, on larger samples cut from the same batch as the respective magnetization samples. The E–J curves, measured at different applied fields and temperatures, have been fitted to a power law with power exponent n (the so-called n-index, which can be regarded as a

measure of the broadening of the transition):

$$E(J, B; T) = E_c\left(\frac{J}{J_c(B; T)}\right)^n \quad (6)$$

with E_c a conveniently chosen electrical field criterion, usually in the range between 10^{-4} and 10^{-5} V m^{-1}, and $J_c(B,T)$ the magnetic field dependence of the critical current density at a given temperature T. The reader can refer to [8] for experimental details. Isothermal magnetization loops have been measured by means of an Oxford MAGLAB vibrating sample magnetometer system (VSM) provided with a 12 T superconducting magnet and a variable temperature insert (VTI). In the VTI, the temperature of the sample can be varied by flowing He gas through a needle valve. Before entering into the sample space, the flowing He gas is heated and its temperature can be controlled by a PID feedback system. The temperature has been measured by two calibrated Cernox thermometers located below the sample space inlet. The sample orientation is with the background magnetic field oriented perpendicularly to the tape flat surface. The full magnetization loops (*major loops*) were produced by sweeping at constant ramp rate the field along different branches, after cooling the sample in zero field (ZFC). At 77 K the background field was ramped: 0 → 7 T; 7 → −2 T; −2 → 2 T; and 2 → 0 T. At 5 K the field was ramped: 0 → 12 T; 12 → −2 T; −2 → 2 T; and 2 → 0 T. *Minor loops* were generated by smaller magnetic field oscillations of ±0.6 T around central values of 3 T at 77 K and 10 T at 5 K.

Minor loops have been collected at different ramp rates: 0.05, 0.1, 0.2, 0.4, 0.6, 0.8 and 1.0 T min^{-1}. These loops have been used to compute the losses.

2.3. Computational details

Finite element (FE) simulations were performed using the H-formulation [7] which shows an excellent ability to converge, combined with an ease imposition of the boundary conditions. In H-formulation, the Ampere law $\nabla \times H = J$ and the Faraday law $\nabla \times E = -\mu_0\mu_r\frac{\partial H}{\partial t}$ are solved in terms of the three components of the magnetic field vector $H = [H_x, H_y, H_z]^T$. In addition we define the current density and the electrical field vectors as $J = [J_x, J_y, J_z]^T$ and $E = [E_x, E_y, E_z]^T$, respectively, which are related by the exponential E–J characteristic of equation (6). Substituting Ampere law and equation (6) into Faraday law we obtain a set of three partial differential equations for the magnetic field H:

$$\mu_0\mu_r\frac{\partial H}{\partial t} + \nabla \times (\rho\nabla \times H) = 0, \quad (7)$$

where

$$\rho = \frac{E_c}{J_c}\left(\frac{J}{J_c}\right)^{n-1}. \quad (8)$$

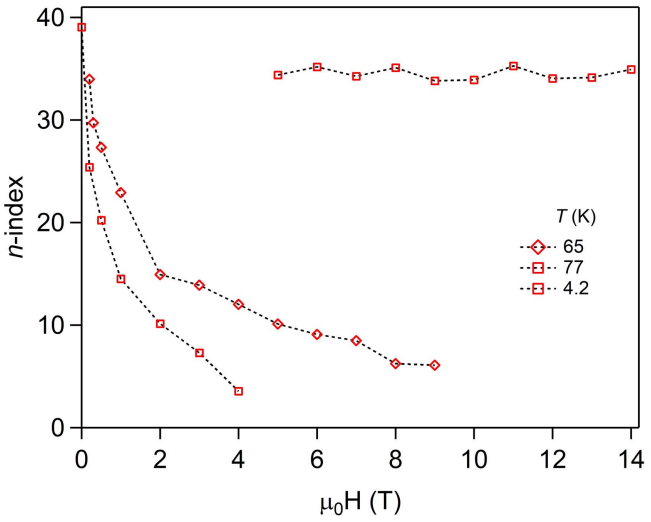

Figure 1. The in-field behavior of n-index of a SuNAM coated conductor measured at different temperatures.

In critical state models, $J_c(B; T)$ can be kept constant (Bean model [9]) or can be defined analytically (fixed pinning [10], square root [11], Kim [12], exponential models [13]). In equation (8), the behavior of the critical current density as a function of field is taken into account by using the experimental $J_c(B)$ curves obtained from the full magnetization cycles within the framework of the critical state model, with the required finite size corrections [7].

Equation (7) is solved applying a time-dependent, uniform magnetic field in the z-direction (i.e., along the thickness direction). Dirichlet boundary conditions are imposed on a boundary area larger than ten times the largest sample dimension. The magnetic field is applied transverse to the strip flat surface and is ramped linearly following the experiment.

The applied field is also varied at different ramp rate. In this paper equation (7) has been solved by the FEM software COMSOL Multiphysics on a workstation equipped with a dual six core Intel Xeon (2.3 GHz, 64 GB RAM).

3. Results and discussion

In table 1, both the I_c values in self-field (sf) and the n-index at 77 K 3 T, and 5 K 10 T are reported. For the evaluation of I_c and the n-index, the experimental E–J curves have been fitted to equation (6) by using $E_c = 10^{-4}$ V m^{-1} and performing the fits in the range 10^{-4}–10^{-3} V m^{-1}. As an example, in figure 1 the n-index are plotted as a function of applied magnetic field, μ_0H, for the SuNAM CC tape. The n-index has been found to be a decreasing function of μ_oH. At higher temperatures, the n-index (sf) values decrease from n = 30–40 to n = 5–10, whereas at 4.2 K the n-index does not change in the field range [5–14] T. In figure 2 the critical current density, $J_c(B)$, is plotted as a function of the applied magnetic field. Here the DC transport measurements and the VSM magnetization measurements are compared. The major magnetization loops have been used to calculate the field dependence of the critical

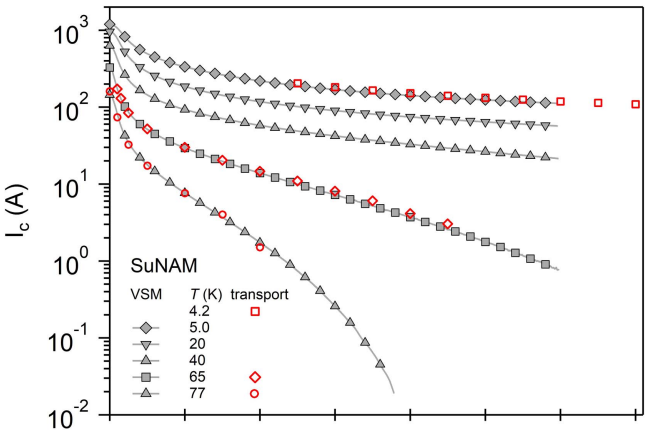

Figure 2. The in-field behavior of critical current of a SuNAM coated conductor measured at different temperatures.

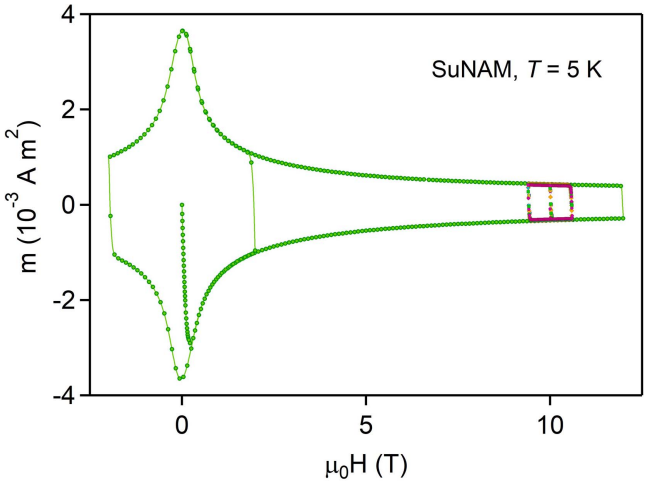

Figure 3. Magnetic moment versus field for a SuNAM CC tape at 5 K. Both major and minor loops are plotted.

current density, $J_c(B)$, to be used in equation (8), through the Bean model formula [7]:

$$J_c(B) = 2\frac{\Delta M(B)}{a\left(1 - \frac{a}{3l}\right)}, \quad (9)$$

where $\Delta M(B)$ (Am^{-1}) is the width of the magnetization hysteresis loop at a given field value B, for increasing and decreasing field, whereas a and l (with $a < l$) are the sample dimensions and d its thickness. In equation (9), the finite size of the measured sample is taken into account by the factor $(1 - a/3\,l)$ [7]. Furthermore to get the zero-frequency limit of J_c (i.e. DC critical current), in calculating $J_c(B)$ from inductive measurements, the field rate dependence was taken into account: we scaled the major loops collected at higher ramp rate to the minor loops collected at 0.05 T min^{-1}. With this procedure, we get a good agreement among the J_c from DC transport and J_c from inductive measurements.

Figures 3 and 4 show the typical magnetization loops measured in the SuNAM ($T = 5$ K) and the SuperPower ($T = 77$ K) CC tapes, along with the minor loops around 10 T

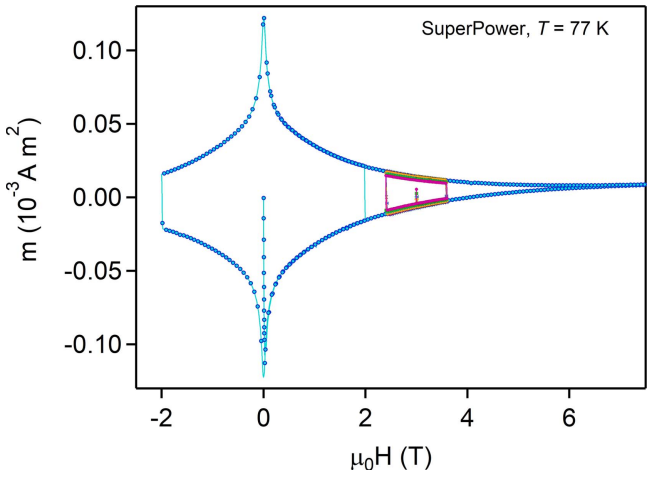

Figure 4. Magnetic moment versus field for a SuperPower CC tape at 77 K. Both major and minor loops are plotted.

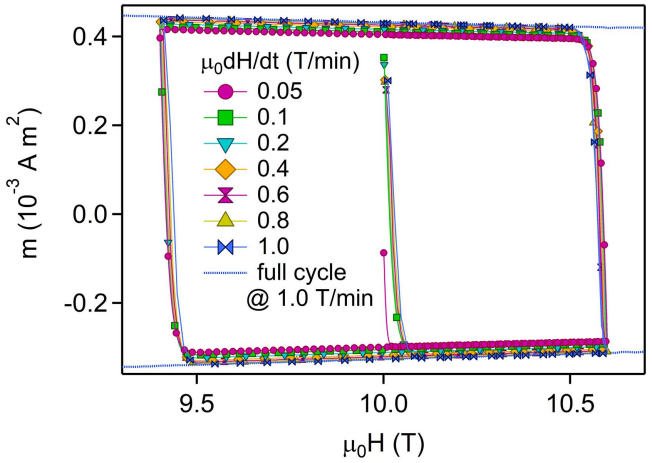

Figure 5. A close view of the minor loops centered at 10 T collected at different ramp rates for a SuNAM tape at 5 K.

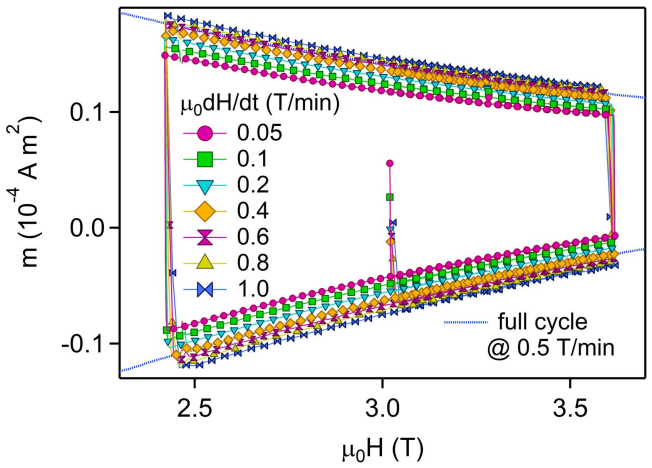

Figure 6. A close view of the minor loops centered at 3 T collected at different ramp rates for a SuperPower tape at 77 K.

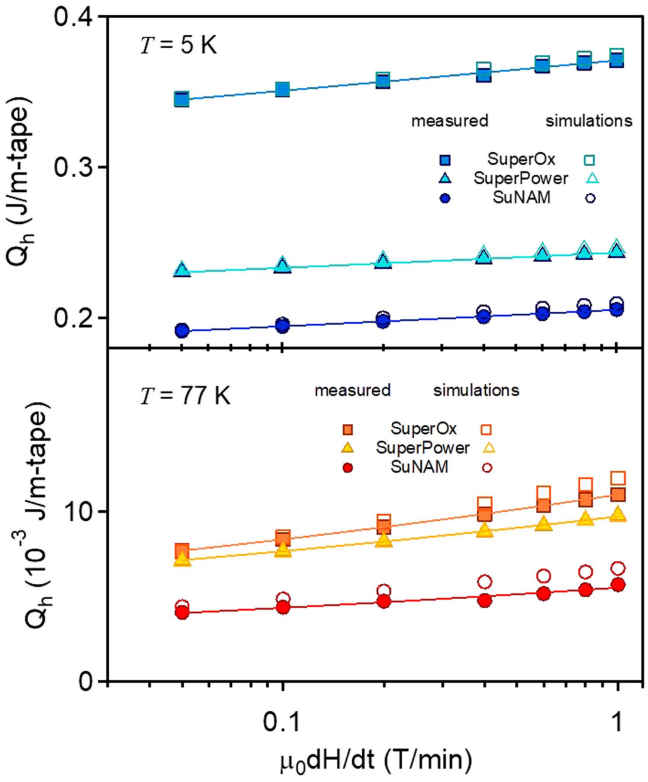

Figure 7. The losses per cycle, $Q_{\rm loss}$, versus ramp rate measured at 5 K, 10 T (top panel) and 77 K, 3 T (bottom panel).

and 3 T, respectively. These minor loops are magnified in figures 5 and 6 where an increase of the magnetization with the increasing field ramp rate can be easily noted. The most direct piece of information provided by these loops is the AC loss per cycle, which is provided by the loop area: assuming that the external field H is uniform over the sample, the hysteretic loss per unit volume per cycle, $Q_{\rm h}$, may be estimated by the integral [14]:

$$Q_{\rm h} = \oint H{\rm d}M = \oint M{\rm d}H. \tag{10}$$

Therefore, using the minor loops measurements, the magnetization loss of the tapes is calculated at 5 and 77 K as the area of the closed loop, for each different ramp rate. By computing the loss per cycle, $Q_{\rm h}$, at different field ramp rates $\dot{B}$ from equation (5) we can obtain the dependences of the measured losses on $\dot{B}$, which can be expressed as:

$$Q_{\rm h}(T, \dot{B}) = k\dot{B}^{1/\nu}, \tag{11}$$

where k is a constant, and ν is a fit parameter representing the n-index obtained from transport measurements.

In figure 7 the effect of the field ramp rate on the hysteresis losses measured at 5 K, 10 T, and 77 K, 3 T is illustrated as solid symbols for the three different samples. The experimental data of figure 7 have been fitted with equation (11): the fit results are reported in table 2, where two different fit procedures are presented. In the first one, the fit parameter ν has been replaced by the n-index experimental value, and k is a free fit parameter. In the second one, we set both k and ν as free parameters. It is worth noting that in this last case we found k, ν values comparable to the ones computed by the first procedure. In addition, to check the goodness of fit and compare among different procedures, we calculated $\chi^2 = \sum_i (y_i^{\rm fit} - y_i^{\rm exp})^2$, where $y_i^{\rm fit}$ is the expected value from equation (11) and $y_i^{\rm exp}$ is the ith experimental data; the values of χ^2 resulting from the second procedure are found to be lower than the χ^2 obtained by keeping $\nu = n$-index.

By a comparison among samples, the SuperOx tape shows the highest losses (and SuNAM the lowest). This is reflected by the k values reported in table 2. Also, the sensitivity to the field ramp rate is found to be proportional to the inverse of the n-index values, as expected. It can be also noticed that the parameter ν is affected by a relatively large error, as small errors in the determination of k results in rather large variation of the slopes of the $Q_{\rm h}(\dot{B})$ curves.

In figure 7, the FE numerical simulations are represented as open symbols. Such simulations reproduce very well the experiments: as it has been recently shown that the $m(H)$ curves can be accurately reproduced by both the ARA model and the H-formulation [7, 15].

The different AC losses values found in the investigated samples cannot be explained by a simple static or CSM, because these models fail to describe systems in which the value of the hysteresis losses (or, equivalently, the V–I characteristic curves) depends on the field-sweeping rate ${\rm d}H/{\rm d}t$ (or ${\rm d}I/{\rm d}t$). In these conditions, the AC losses are influenced by many other physical parameters, including frequency, amplitude of field, n-index values, type of substrate and geometric factors. In our samples, the substrates are non-magnetic at operating temperatures, so they should not play a significant role in measured AC losses. On the contrary, the presence of APCs could have a great impact on the flux dynamics at high fields, and this could be reflected in the values of the n-indexes, which are found to be higher in the SuperPower tape. To confirm this conjecture, however, it is necessary to carry out dedicated experiments of flux dynamics (magnetization relaxation or AC susceptibility), which go beyond the scope of the present work.

It is noticeable that the combination of DC measurements (transport or magnetic) and numerical simulations can provide two simple procedures to evaluate the hysteresis losses as a function of the ramp rate.

If only DC transport data are available, from the experimental data one can get the $J_{\rm c}(B)$ dependence and the n-values at a given field range and:

(a) from the I–V curves, evaluate $J_{\rm c}$ and n-indexes as a function of applied field;
(b) by using $J_{\rm c}(B)$ and $n(B)$ from (a), simulate the magnetization loops with the FE method described in section 2.3;
(c) calculate the area of the simulated loops by using equation (10);
(d) carry out a fit to equation (11) by keeping ν frozen to the measured n-index.

However, whenever magnetic data are available, a different method can be applied.

Table 2. Results of the fits to equation (11). The first set of parameters have been obtained by using the constrain $\nu = n$-index. In the second set, both k and ν are free parameters.

	SuNAM		SuperPower		SuperOx	
Parameters	5 K, 10 T	77 K, 3 T	5 K, 10 T	77 K, 3 T	5 K, 10 T	77 K, 3 T
k (J s$^{1/n}$ T$^{-1/n}$/m-tape)	0.2329 ± 0.0005	$(9.9 \pm 0.2) \times 10^{-3}$	0.2655 ± 0.0003	$(14.98 \pm 0.03) \times 10^{-3}$	0.4149 ± 0.0006	$(21.1 \pm 0.3) \times 10^{-3}$
n-index	34.0 ± 0.3	7.3 ± 0.5	47.8 ± 0.4	9.5 ± 0.7	37.3 ± 0.3	6.6 ± 0.4
$\chi 2$ (J^2 m^{-2})	9.2×10^{-6}	2.7×10^{-7}	3.1×10^{-6}	1.2×10^{-8}	1.0×10^{-5}	6.2×10^{-7}
k (J s$^{1/n}$ T$^{-1/n}$/m-tape)	0.2261 ± 0.0003	$(8.5 \pm 0.5) \times 10^{-3}$	0.2618 ± 0.0002	$(14.8 \pm 0.1) \times 10^{-3}$	0.409 ± 0.002	$(17.88 \pm 0.03) \times 10^{-3}$
ν-index	41.9 ± 0.5	9 ± 1	54.8 ± 0.3	9.8 ± 0.2	41 ± 1	8.41 ± 0.02
$\chi 2$ (J^2 m^{-2})	1.0×10^{-7}	1.1×10^{-7}	2.7×10^{-8}	8.0×10^{-9}	4.6×10^{-6}	3.3×10^{-10}

1. Measure a major loops at the lowest field ramp rate (if ramping at higher ramp rates, a correction factor must be applied).
2. Measure isothermal minor loops around a given background field.
3. Calculate the area of the simulated loops by using equation (10).
4. Carry out a fit to equation (11) with two fit parameters, k and ν.

The methods described in this work can be used to extrapolate the losses at higher field ramp rates, not experimentally accessible with a VSM. There are two ways available for extrapolating: by means of equation (11), or by carrying out FE simulations.

For example, at $T = 5$ K we calculated from equation (11) the following percentage increases of Q_h with respect to the reference value at 0.05 T min^{-1} (8×10^{-4} T s^{-1}) for the considered samples: 14%–19% at 1 T s^{-1}; 17%–24% at 5 T s^{-1}; and 19%–26% at 10 T s^{-1}. Similarly, at $T = 77$ K we obtained: 106%–132% at 1 T s^{-1}; 143%–181% at 5 T s^{-1}; 161%–205% at 10 T s^{-1}. At both temperatures, the sensitivity to the field ramp rate is higher in SuperOx, whereas the SuperPower tape showed the lowest Q_h percentage increase. Alternatively, one can directly perform FE calculations at higher field ramp rates.

4. Conclusion

The hysteretic losses have been studied as a function of the frequency in three different commercial 2 G HTS tapes, either by experimental and numerical simulations. The experiments where performed at 3 T, 77 K and 12 T, 5 K. As previously observed [3] at lower applied field values, also in this range of magnetic field and temperatures a typical power-law behavior $Q_h(T, \dot{B}) = k\dot{B}^{1/\nu}$ has been observed, where the exponent ν may be determined either by transport measurements or by means of a fit procedure.

The use of combined DC experiments with FE numerical simulation can provide a tool for computing the hysteretic losses at different frequencies, even outside the available range for the experimental field rates.

Acknowledgments

The authors thank the companies SuNAM, SuperOx, and SuperPower for providing the samples, R Viola for experimental assistance, and A Saggese for useful discussions.

ORCID iDs

G De Marzi https://orcid.org/0000-0002-5752-2315
G Iannone https://orcid.org/0000-0001-8347-7549
U Gambardella https://orcid.org/0000-0003-0551-2120

References

[1] Rey C M (ed) 2015 *Superconductors in the Power Grid: Materials and Applications* (*Woodhead Publishing Series in Energy* vol 65) (Amsterdam: Elsevier)
[2] Grilli F and Kario A 2016 How filaments can reduce AC losses in HTS coated conductors: a review *Supercond. Sci. Technol.* **29** 083002
[3] Polak M, Kvitkovic J, Mozola P, Usak E, Barnes P N and Levin G A 2007 Frequency dependence of hysteresis loss in YBCO tapes *Supercond. Sci. Technol.* **20** S293
[4] Bean C P 1962 Magnetization of hard superconductors *Phys. Rev. Lett.* **8** 250
[5] Brandt E H and Indenbom M 1993 Type-II-superconductor strip with current in a perpendicular magnetic field *Phys. Rev.* B **48** 12893
[6] Banno N and Amemiya N 1999 Analytical formulae of coupling loss and hysteresis loss in HTS tape *Cryogenics* **39** 99
[7] Iannone G, Farinon S, De Marzi G, Fabbricatore P and Gambardella U 2015 Modeling experimental magnetization cycles of thin superconducting strips by finite element simulations *IEEE Trans. Appl. Supercond.* **25** 8200107
[8] De Marzi G, Celentano G, Augieri A, Muzzi L, Tomassetti G and Della Corte A 2015 Characterization of the critical current capabilities of commercial REBCO coated conductors for a HTS cable in conduit conductor *IEEE Trans. Appl. Supercond.* **25** 6602804
[9] Bean C P 1964 Magnetization of high-field superconductors *Rev. Mod. Phys.* **36** 31
[10] Ji L, Sohn R H, Spalding G C, Lobb C J and Tinkham M 1989 Critical-state model for harmonic generation in high-temperature superconductors *Phys. Rev.* B **40** 10936
[11] Leblanc D and LeBlanc M A 1992 AC-loss valley in type-II superconductors *Phys. Rev.* B **45** 5443
[12] Kim B, Hempstead C F and Strnad A R 1962 Critical persistent currents in hard superconductors *Phys. Rev. Lett.* **9** 306
[13] Fietz W A, Beasley M R, Silcox J and Webb W W 1964 Magnetization of superconducting Nb-25% Zr wire *Phys. Rev.* **136** A335
[14] Wilson M N 1983 *Superconducting Magnets* (Oxford: Clarendon)
[15] Farinon S, Iannone G, Fabbricatore P and Gambardella U 2017 Numerical modeling of critical-state magnetization in type-II superconducting cylinders under parallel and transverse magnetic field *Cryogenics* **81** 107